Geosci. Model Dev., 14, 2205–2220, 2021
https://doi.org/10.5194/gmd-14-2205-2021

Geoscientific Model Development
Open Access
EGU

A new Lagrangian in-time particle simulation module (Itpas v1) for atmospheric particle dispersion

Matthias Faust[1], **Ralf Wolke**[1], **Steffen Münch**[2], **Roger Funk**[2], **and Kerstin Schepanski**[1]

[1]Leibniz Institute for Tropospheric Research (TROPOS), Permoserstr. 15, 04318 Leipzig, Germany
[2]Leibniz Centre for Agricultural Landscape Research (ZALF), Eberswalder Str. 84, 15374 Müncheberg, Germany

Correspondence: Matthias Faust (faust@tropos.de)

Received: 19 October 2020 – Discussion started: 5 November 2020
Revised: 13 February 2021 – Accepted: 9 March 2021 – Published: 27 April 2021

Abstract. Trajectory models are intuitive tools for airflow studies. But in general, they are limited to non-turbulent, i.e. laminar flow, conditions. Therefore, trajectory models are not particularly suitable for investigating airflow within the turbulent atmospheric boundary layer. To overcome this, a common approach is handling the turbulent uncertainty as a random deviation from a mean path in order to create a statistic of possible solutions which envelops the mean path. This is well known as the Lagrangian particle dispersion model (LPDM). However, the decisive factor is the representation of turbulence in the model, for which widely used models such as FLEXPART and HYSPLIT use an approximation. A conceivable improvement could be the use of a turbulence parameterisation approach based on the turbulent kinetic energy (TKE) at high temporal resolution. Here, we elaborated this approach and developed the LPDM Itpas, which is coupled online to the German Weather Service's mesoscale weather forecast model COSMO. It benefits from the prognostically calculated TKE as well as from the high-frequency wind information. We demonstrate the model's applicability for a case study on agricultural particle emission in eastern Germany. The results obtained are discussed with regard to the model's ability to describe particle transport within a turbulent boundary layer. Ultimately, the simulations performed suggest that the newly introduced method based on prognostic TKE sufficiently represents the particle transport.

1 Introduction

We are living in a polluted world. Altogether, our industry, our mobility and our agriculture cause particulate matter emissions (Taiwo et al., 2014; Pant and Harrison, 2013; Kjelgaard et al., 2004) that decrease air quality and thus impact on human health in affected regions (Kim et al., 2015). But natural aerosol emissions like from soil erosion by wind can also result in dusty haze plumes or mature dust storms which may locally cause poor air quality (Goudie, 2014). In central Europe, dust emissions can occur in agricultural environments. These are driven on the one hand by wind erosion and on the other hand by activities like tillage and harvest (Goossens, 2004). Wind erosion occurs predominantly in plains and on sandy soil under favourable conditions such as high wind speeds, low vegetation cover and low soil moisture. On average the soil loss by wind erosion in Europe is estimated to be $0.53\,\mathrm{t\,ha^{-1}\,yr^{-1}}$ (Borrelli et al., 2016), but extreme wind erosion events can be associated with a soil loss of more than $100\,\mathrm{t\,ha^{-1}}$ (Funk and Reuter, 2006). Furthermore the increasing drought conditions as a result of the climate crisis (Samaniego et al., 2018; Marx et al., 2018) can be expected to amplify soil loss by wind erosion. Other than wind erosion, dust emission by tillage is not a function of the wind velocity. Since the particles are lifted mechanically the emission depends mainly on the tool used and the soil moisture (Funk et al., 2008). Goossens (2004) estimated 4-times-higher dust emissions caused by tillage operations than by natural wind erosion. Whereas wind erosion has been considered in aerosol–atmosphere models for several decades (e.g. Joussaume, 1990; Tegen et al., 2002; Huneeus et al., 2011),

dust emission driven by agricultural activities has so far been underrepresented.

But assuming we know the source of the pollution, e.g. the tilling tractor, the central remaining questions for air quality studies are (1) where is it transported to and, consequently, (2) which regions are affected. Thereby, not only the transport direction but also the altitude and the concentration is of relevance. To shed light on the air travel of a polluted (aerosol-loaded) air mass, in general the pathway of an imaginary air parcel is traced through the atmosphere. In other words, its trajectory is determined. This trajectory is then considered as representative for the pathway of the associated aerosol plume.

In order to estimate the air parcel's route through the atmosphere, trajectory models use gridded wind fields as provided by numerical weather prediction (NWP) models for their calculations. But, within the atmospheric boundary layer (ABL), wind and the air flow are characterised by small-scale and micro-scale turbulent eddies, and it is challenging to track the motion of individual air parcels due to the frequent change in direction (Stohl, 1998). Since NWP models are usually not able to resolve such small-scale processes, it is impossible to calculate an accurate trajectory in a turbulent boundary layer.

A common approach for trajectory-based dispersion studies within the ABL is the application of Lagrangian particle dispersion models (LPDMs). Therefore, the main idea is to handle the deviations due to turbulence as a stochastic deviation from the mean transport path. So, a single trajectory becomes one possible solution of the transport in the chaotic system, and an extensive set of trajectories statistically describes the range of possible pathways, which can also be seen as particle dispersion. In this term, particles can be considered either as tracers or simple air parcels, as well as aerosol particles with more complex attributes such as density and size.

Widely used LPDMs like FLEXPART (Pisso et al., 2019; Stohl et al., 2005) and HYSPLIT (Draxler and Hess, 1998; Stein et al., 2015) are designed to simulate tracer transport on a global scale, but there are also mesoscale applications like FLEXPART-WRF (Brioude et al., 2013). To characterise and account for the boundary layer turbulence, these models use a rough estimate of turbulence based on boundary layer depth and atmospheric stability (Hanna, 1982). As meteorological input (e.g. wind, temperature), FLEXPART and HYSPLIT use output fields from global forecast or reanalysis models, which are typically available at a time increment of a few hours (typically 3-hourly or 6-hourly). However, in contrast to the output interval of a few hours, the trajectory calculation should be performed at high temporal resolution (time steps of minutes or less) in order to fulfil the Courant–Friedrichs–Lewy (CFL) condition (Seibert, 1993). Consequently, an interpolation between two consecutive times for which the meteorological input fields are available becomes necessary. This is a crucial issue, especially for small-scale applications at short timescales.

One approach to avoid the temporal interpolation is coupling the trajectory calculation with the NWP model directly and thus circumventing the import of (external) meteorological fields to the LPDM. This so-called online coupling (or inline coupling) allows all necessary parameters like wind to be updated with every NWP model time step, typically every few seconds. Compared to the above-described offline-driven system, this approach results in more accurate trajectories like the study of Miltenberger et al. (2013) has shown. But there are also disadvantages: online coupled model systems are only able to calculate forward in time; the calculation of backward trajectories is not possible with this approach. And since a NWP model always has to run just in time with the trajectory computation, additional computational resources are needed.

However, to make an accurate prediction of transport and dispersion processes within the atmospheric boundary layer it is worth coupling the LPDM to a NWP model online. This technique is used in the WRF application WRF-HYSPLIT (Ngan et al., 2015), where HYSPLIT runs just in time with WRF. The authors found that the online coupled HYSPLIT version produces better results than the offline version for applications with small temporal and spatial scale (Ngan et al., 2015, 2018). In their study, WRF-HYSPLIT uses the online coupling mainly to avoid the temporal interpolation of the winds. But information on the state of the atmosphere may also be useful to improve the estimation of the turbulence in the LPDM, in particular the turbulent kinetic energy (TKE) that is handled as a prognostic variable in many NWP models.

Here, we integrate the TKE-based approach to the standard trajectory module of Miltenberger et al. (2013), which is included in the state-of-the-science NWP model COSMO developed at the German Weather Service (Deutscher Wetterdienst, DWD) (Baldauf et al., 2011). Our approach makes use of the three-dimensional TKE-based turbulence scheme (Doms et al., 2011), which provides the prognostic TKE, and the horizontal and vertical diffusion coefficient of momentum. We further developed a dust emission scheme accounting for mechanical dust emission in agriculture based on measurement data (Münch et al., 2020) and implemented a probabilistic dry deposition scheme (Panitz et al., 1994).

In a nutshell, the new LPDM module Itpas (In time particle simulation) now allows for an improved representation of individual trajectories in a turbulent boundary layer. Furthermore, Itpas can handle weightless air parcels as well as aerosol particles like mineral dust. Currently, Itpas is used with the COSMO version `V5.04e`.

The present paper is structured as follows: first, we introduce the LPDM Itpas, the way it was developed and the physics it uses. Afterwards, we present a showcase for a possible application. Here, we used Itpas to simulate the dispersion of a soil particle plume emitted by a tractor.

2 Methods

2.1 Model description

The starting point of our development was the trajectory module developed by Miltenberger et al. (2013). The software package consists of two files: `data_part` and `src_part`. The first file provides information on parameters, global variables and namelist variables; the file `src_part` contains the LPDM code. There is only a weak link between Itpas and COSMO. We only added a switch to activate the particle module and call statement in the COSMO main routine.

The particle model is called at the end of every COSMO time step and reads in the most recent wind and turbulence field arrays. Every particle is handled individually by the LPDM, so, as illustrated in Fig. 1, the overall structure is a loop over every active particle. A typical call performs the following steps: first, the particle transport by the mean wind is investigated. For describing the particle's vertical motion, the settling velocity is taken into account for particles with a mass. Afterwards the turbulent disturbance is calculated. Therefore, it is important to know if the particle resides inside the ABL or above:

- Inside the ABL, the turbulent part of the wind velocity is calculated with a general approach which is presented in detail in the next section. The turbulent wind velocity is integrated with an Euler forward step. This leads to the turbulent part of the particle motion which is added to the mean particle motion. Since the particle is not allowed to leave the boundary layer directly, the model checks if the particle is still inside the boundary layer after the motion. If not, the particle is reflected back into the ABL. If the particle hits the surface, it is decided whether the particle is removed by dry deposition or whether it is reflected back into the atmosphere, based on a probability function (see Eq. 17).
- If the particle is above the ABL at the beginning of the calculation, a reduced approach is used to investigate the turbulent part of the particle motion. Afterwards it is checked whether the particle hits the surface, just like described above.

At the end of the loop, the particle is marked either as "dead" or "alive". The particle can "die" because of dry deposition and consequently the removal from the atmosphere, but also by leaving the model domain. A "dead" particle is frozen at its last position until the end of the simulation. All particles that stay "alive" are ready to run through the particle loop at the next time step again.

Itpas is controlled by a namelist and a start file. In the namelist, important parameters can be defined, like the maximum number of particles, paths for input and output, the seed for the random number generator and the output increment. The start file defines the particle start positions and attributes like size and density. It is possible to define continuously emitting sources and start points that release multiple (thousands of) particles. More details on the model set-up can be found in the ReadMe file which is included in the Supplement.

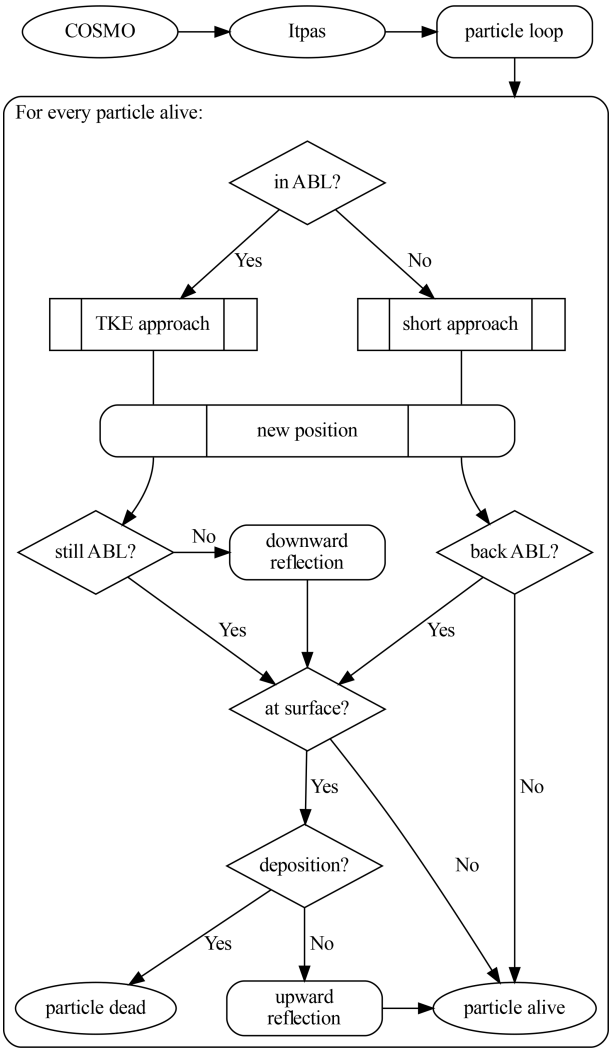

Figure 1. Flow chart of the transport algorithm.

The output is written in NetCDF format (Unidata, 2020) and contains the trajectory positions for every output step as well as the attributes size and density. One of the biggest advantages of the LPDM compared to the Eulerian system is the ability to produce strong gradients and sharp edges of a particle plume. Therefore we avoided transforming the trajectories into gridded data (e.g. trajectory-density). But if necessary this can be done in the post-processing.

2.2 Model physics

The Reynolds average of the wind velocity $\boldsymbol{u} = \overline{\boldsymbol{u}} + \boldsymbol{u}'$ describes the true wind velocity $\boldsymbol{u}$ as the superposition of the mean wind velocity $\overline{\boldsymbol{u}}$ with a turbulent disturbing $\boldsymbol{u}'$. Also in the turbulent boundary layer, the major part of the transport is due to advection as a function of the mean wind. For the advective transport, we use the iterative integration scheme (Petterssen, 1956) from the online trajectory module of Miltenberger et al. (2013).

To determine the turbulent proportion of the wind velocity we use a generalised form of Langevin's equation (Lemons and Langevin, 2002).

$$\boldsymbol{u}' = \boldsymbol{a}(\boldsymbol{x}, \boldsymbol{u}, t)\mathrm{d}t + \boldsymbol{b}(\boldsymbol{x}, \boldsymbol{u}, t)\boldsymbol{\xi} \tag{1}$$

The first term of this equation describes the conservation of momentum. The coefficient $\boldsymbol{a}$ is a memory function that depends on the particle's position ($\boldsymbol{x}$) and velocity ($\boldsymbol{u}$) at a specific time (t). The second term gives a random displacement. The coefficient $\boldsymbol{b}$ contains the potential strength of the turbulence; $\boldsymbol{\xi}$ is a normal distributed random number with a mean value of zero and a standard deviation of one. In that way, every particle gets a random push with the mean strength of the turbulence. The general solution for this selection problem was established by Hall (1975). Looking at $\boldsymbol{u}'$ for the discrete time step $t+1$, Langevin's equation is set up as follows:

$$\boldsymbol{u}'_{t+1} = \boldsymbol{a}\boldsymbol{u}'_t + \boldsymbol{b}\boldsymbol{\xi}. \tag{2}$$

The parameter $\boldsymbol{a}$ is defined as the correlation function $\boldsymbol{R}$ (Hall, 1975):

$$\boldsymbol{a} = \boldsymbol{R} = \exp\left(-\frac{\mathrm{d}t}{\boldsymbol{\tau}_\mathrm{L}}\right). \tag{3}$$

It describes the connection of the model time step $\mathrm{d}t$ and $\boldsymbol{\tau}_\mathrm{L}$, the characteristic timescale for the Lagrangian dispersion process. The correlation function expresses the following: if $\mathrm{d}t >> \tau_{\mathrm{L};u,v,w}$ then there is no further dependency between the velocities $\boldsymbol{u}'_{t+1}$ and $\boldsymbol{u}'_t$. The parameter $\boldsymbol{b}$ is defined as follows:

$$\boldsymbol{b} = \boldsymbol{\sigma}\sqrt{1 - \boldsymbol{R}^2}, \tag{4}$$

with $\boldsymbol{\sigma}$ the standard deviation of the wind (Hall, 1975).

Now parametrisations for $\boldsymbol{\sigma}$ and $\boldsymbol{\tau}_\mathrm{L}$ are necessary to solve the equation of motion. A common approach uses the TKE ($\overline{e}$), which describes how much kinetic energy is available to generate atmospheric turbulence. Kinetic energy is well known as $\frac{E_\mathrm{kin}}{m} = \frac{1}{2}v^2$. Based on this the kinetic energy of the turbulent wind fraction is defined as follows:

$$\overline{e} = \frac{1}{2}\left(\overline{u'^2} + \overline{v'^2} + \overline{w'^2}\right), \tag{5}$$

with the turbulent wind u', v' and w' of the spacial directions. The variance of a variable is defined as the average of the squared fluctuation $\sigma_u^2 = \overline{u'^2}$ (Stull, 2012). This allows the standard deviation of the wind velocity to be parametrised with the TKE,

$$\boldsymbol{\sigma} = \sqrt{2\boldsymbol{m}\overline{e}}. \tag{6}$$

The m_i factors ($m_i \in \mathbb{R}$ with $0 \geq m_i \geq 1$ and $\sum m_i = 1$; $i = \{u, v, w\}$) describe the weighting of the TKE in each spatial direction, which has a strong dependence on the ambient wind velocity and the atmospheric stratification. In our approach we define the m_i values as the fractions of the mean wind on every model time step.

$$m_i = \frac{|i|}{|\overline{\boldsymbol{u}}|} \tag{7}$$

For the parametrisation of the characteristic timescale, the diffusion coefficient of momentum ($\boldsymbol{K}_\mathrm{m}$) is used,

$$K_{\mathrm{m},x} = \frac{1}{2}\sigma_x^2\frac{\overline{u}}{x}. \tag{8}$$

Here, σ_x^2 is the variance of a spatially dispersed tracer. Taylor (1922) showed that σ_x^2 can be expressed as follows:

$$\sigma_x^2 = 2\sigma_u^2\tau_{\mathrm{L},u}t, \tag{9}$$

under the condition that time $t \gg \tau_{\mathrm{L},u}$. The combination of Eqs. (8) and (9) with $t = \frac{x}{\overline{u}}$ leads directly to the parametrisation of the characteristic timescale,

$$\boldsymbol{\tau}_\mathrm{L} = \frac{\boldsymbol{K}_\mathrm{m}}{\boldsymbol{\sigma}^2}. \tag{10}$$

Now, all parts of the turbulent particle motion are parametrised with available variables of the NWP model. This allows Eqs. (2), (3) and (4) to be combined into the general solution (11), which can be solved with the parametrisations (6) and (10):

$$\boldsymbol{u}'(t) = \boldsymbol{R}\boldsymbol{u}'(t - \Delta t) + \boldsymbol{\sigma}\sqrt{1 - \boldsymbol{R}^2}\boldsymbol{\xi} + (1 - R_w)\tau_{\mathrm{L},w}\left(\frac{\partial\sigma_w^2}{\partial z} + \frac{\sigma_w^2}{\rho}\frac{\partial\rho}{\partial z}\right)\begin{pmatrix}0\\0\\1\end{pmatrix}. \tag{11}$$

For the vertical turbulence, there is a correction necessary that takes into account the vertical variability of the density (Stohl and Thomson, 1999) and the profile of the standard deviation (Legg and Raupach, 1982).

At the top of the boundary layer, there is a hard transition of the wind regime. Inside the boundary layer, there is a turbulent wind regime with possibly strong vertical velocities. Above the boundary layer, the turbulent part of the particle motion is strongly reduced. Therefore a simplified approach can be used for which the standard deviation of the turbulent wind is described by the diffusion coefficient per time

step $\boldsymbol{\sigma} = \sqrt{\frac{\boldsymbol{K}_\mathrm{m}}{\mathrm{d}t}}$ (Stohl et al., 2005), which leads to a turbulent wind velocity of

$$\boldsymbol{u'} = \sqrt{2\frac{\boldsymbol{K}_\mathrm{m}}{\mathrm{d}t}}\xi. \tag{12}$$

The model is designed to describe the airborne transport of aerosol particles like mineral dust. As these particles settle by gravity, we need to introduce the gravitational settling velocity (v_g), which depends on the particle size and therefore on the Reynolds number (Re). For small Reynolds numbers, v_g can be calculated directly (Hinds, 1999):

$$v_\mathrm{g} = \frac{\rho_\mathrm{p} d_\mathrm{p}^2 g C_\mathrm{c}}{18\eta} \quad \text{for } Re \leq 0.4, \tag{13}$$

with the density and diameter of the particle ρ_p and d_p, the gravity g, the dynamic viscosity of air η, and slip correction factor (Cunningham correction) C_c. For particle settling under conditions of high Reynolds numbers ($Re > 0.4$), an empirical approach is used (Hinds, 1999):

$$v_\mathrm{g} = \left(\frac{\eta}{\rho_\mathrm{air} d_\mathrm{p}}\right) \exp\left(-3.07 + 0.9935J - 0.0178J^2\right), \tag{14}$$

where

$$J = \ln\left(\frac{4\rho_\mathrm{p}\rho_\mathrm{air} d_\mathrm{p}^3 g}{3\eta^2}\right). \tag{15}$$

Particles near the surface may be removed by dry deposition. Thereby the dry deposition velocity v_d is important, which describes the velocity of the diffusion near the surface. Following Zhang et al. (2001) it is defined as follows:

$$v_\mathrm{d} = v_\mathrm{g} + \frac{1}{R_\mathrm{a} + R_\mathrm{s}}, \tag{16}$$

with the atmospheric resistance R_a and the surface resistance R_s. Since motion is already calculated individually for each particle, it is useful to handle the deposition individually as well. Therefore we use the deposition probability W_d. It describes how likely it is that a particle remains at the ground once it has hit the surface. An approach for this can be found in Panitz et al. (1994):

$$W_\mathrm{d} = \frac{\sqrt{2\pi}\frac{v_\mathrm{d}}{\sigma_0}}{F_\mathrm{g} + \sqrt{\frac{\pi}{2}}\frac{v_\mathrm{d}}{\sigma_0}}. \tag{17}$$

Here $\sigma_0 = 2.5u_\star\sqrt{m_\mathrm{w}}$ is the standard deviation of the vertical wind right at the surface, where $u_\star$ is the friction velocity. F_g describes the gravitational part of the dry deposition with $\gamma = v_\mathrm{g}\left(\sqrt{2}\sigma_0\right)^{-1}$ and $\mathrm{erf}(\gamma)$ the error function of γ,

$$F_\mathrm{g} = \sqrt{\frac{\pi}{2}}\frac{v_\mathrm{g}}{\sigma_0} + \frac{e^{-\gamma^2}}{1 + \mathrm{erf}(\gamma)}. \tag{18}$$

3 Model application

The above-described LPDM was developed in order to trace mineral dust particles emitted from arable land during tillage. Other than wind erosion of mineral dust, which is described as a function of the near-surface wind speed, soil particles are entrained mechanically into the atmosphere during agricultural activities on the field like tillage, traffic, fertilisation and harvest. These so-called fugitive emissions may occur independent of the ambient wind speed, but, nevertheless, the ABL dynamics determine the particles' lifetime in the atmosphere. Emission potentials for farming activities have been determined in numerous studies (Funk et al., 2008; Holmén et al., 2001; Kjelgaard et al., 2004), but the further fate of the emitted quantities is still relatively unclear. Here, we use Itpas to examine the role of the diurnal ABL development in the dispersion of soil dust and organic manure dust particles, which were emitted mechanically during typical field work: the application of dry fertiliser with a spreader and the subsequent incorporation of the fertiliser with a cultivator. The field work was carried out in the framework of the SOARiAL (Spread of antibiotics resistance in an agrarian landscape) project (Thiel et al., 2020), during which airborne particle concentrations were measured as described by Münch et al. (2020).

3.1 Field experiment

The experiment took place at an agricultural field near Müncheberg, Germany, approximately 50 km east of Berlin, on 31 May 2017 (Münch et al., 2020; Thiel et al., 2020). During this day, the weather over eastern Germany and western Poland was dry with some shallow cumulus clouds. During the experiment a gentle breeze ($\sim 5\,\mathrm{m\,s^{-1}}$) blew from the northwest.

The experiment was carried out as follows: a tractor drove in parallel lines across the field, orientated perpendicular to the ambient wind (Fig. 2). Downwind, beside the field, the particle number concentration was measured with two vertically stacked Environmental Dust Monitors (EDM 164, GRIMM-Aerosol Technique) at two different inlet heights (1.5, 3.8 m). The EDMs measured particle number concentrations at 31 size bins ranging from 0.25 to 32 µm.

The experiment was divided into two parts:

EXP1 Dried chicken manure was spread on the field as fertiliser from 08:50 to 09:45 UTC.

EXP2 The fertiliser was incorporated into the soil by a cultivator from 11:40 to 12:30 UTC.

During both experiments, a particle plume rose behind the tractor; although the tilling entrained far more particles into the atmospheric boundary layer than the fertiliser spreading. While the measurements provide information on the particle number and size distribution and thus characterise the particle plume developing, the question remains of how long

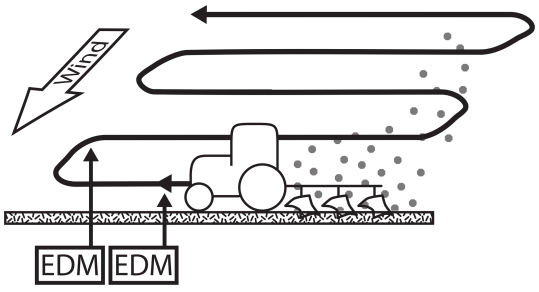

Figure 2. Sketch of the experimental set-up: the tractor drives in parallel orientated tracks over the field. Downwind the emitted particle plume is measured by two vertically stacked Environmental Dust Monitors.

these particles will remain in the atmosphere and how they will be dispersed. As it can be assumed that the turbulent nature of the convective daytime boundary layer is relevant to the accurate simulation of the dispersion, these two experiments were simulated in order to showcase the strength of our online coupled LPDM Itpas driven by prognostic TKE.

3.2 Source function

In the framework of this study, dust entrainment was mechanically driven by the tools pulled behind the tractor and not by wind. A source function was obtained based on the measured particle concentrations in order to describe the dust particle uplift. Therefore we created an idealised version of the particle plume for which we use the EDM data to define a vertical profile of particle concentration. The profile was then multiplied by a half-sphere in order to get a 3D concentration field with which we can define the particle start points for the Itpas simulation. Thereby, the particle concentration determines the number of the trajectories starting at the respective point. The particle size is used to assign the corresponding particle properties such as the diameter, which is relevant for determining the particle's residence time in the atmosphere.

In particular, we defined a vertical profile that represents the centre of the tractors particle plume (Fig. 3a). Therefore we used the observation data of the moment when the tractor passed by the measurement device as close as possible. Besides the values of the two measurement heights (inlet heights) two additional assumptions are necessary. First, the particle concentration at ground level corresponds to that at 1.5 m. In general, it seems to be more realistic that the particle concentration is higher at ground level than at 1.5 m, especially for coarse particles. But since there is no information about the near-surface concentration available, this conservative assumption is the best choice. Second, the particle concentration becomes zero at a height of 5 m. The plume height also depends on multiple properties such as atmospheric conditions, soil texture, soil moisture and the kind of tool pulled by the tractor. But, based on observations and photo documentation of the experiment, 5 m seems to be a good estimate, at least for this specific case. With these four initial values (two measured and two assumed), the vertical particle number concentration profile of the plume centre was created with a polynomial fit (Fig. 3a).

Then a normalised spherical concentration field with a radius of 5 m was multiplied with the vertical profile, resulting in a three-dimensional field of the particle concentration (Fig. 3b). From this, the total number of particles inside the plume is determined. For the measurements in the case study that were some billion particles. This number of particles cannot be handled individually within the model simulation and thus needed to be downscaled. Here we chose a scaling factor of 2×10^{-7}. So, one particle in the model represents five million measured particles. In total, we used $\sim 100\,000$ particles in EXP1 and $\sim 270\,000$ particles in EXP2. All particles are assigned to random positions in the idealised cloud under the condition that particle distribution matches the concentration field (Fig. 3c). This analysis was performed for each bin provided by the EDM data, so the particle size distribution in the model corresponds to the measurements. An extended version of Fig. 3 with profiles and concentration fields for the individual bins can be found in the Supplement (Figs. S1–S4). With this method we created a bell-shaped cloud of individual particles that we used as model input. Please note that the exact shape of the particle source becomes less important with increasing transport distance.

3.3 Simulations

For EXP1 and EXP2 individual simulations were performed. As input data for the NWP model, we used reanalysis data from COSMO, provided by the German weather service. The model domain covers an area from eastern Germany to central Poland including the cities of Berlin and Poznań (lower left corner: 51° N, 12° E; upper right corner: 54.4° N, 19.3° E) and has a size of 167 × 150 grid cells with a spatial grid spacing of 2.8 km and 50 vertical levels.

In the first simulation EXP1 (the spreading of the dry fertiliser), the particles were emitted during the 55 min time span from 08:50 to 09:45 UTC at the position 52.477° N, 14.177° E. In EXP2 (incorporation of the fertiliser with a cultivator), the particles were emitted at the same position for 50 min from 11:40 to 12:30 UTC. Local time is UTC+2. For both experiments, a continuous release of particles was assumed during the time of emission.

Analysing the simulation output, we focused in particular on the horizontal dispersion, the deposition and the vertical mixing as these three aspects may provide best insights into the model's capability to capture the dispersion of particles within a turbulent boundary layer. These parameters are presented in Figs. 4 and 5, each with panel (a) showing the trajectories indicating the dispersion from a bird's eye perspective. Each line represents the path of one simulated particle trajectory. Panel (b) shows the same map, but with points indicating where particles were deposited. Panel (c) shows the

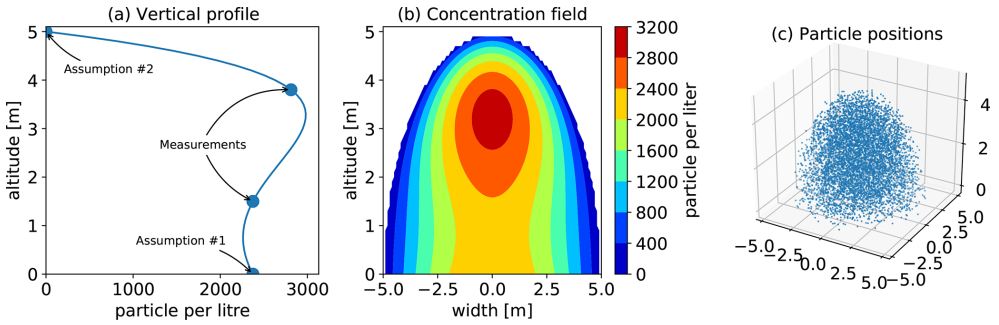

Figure 3. Example construction of an idealised particle cloud. **(a)** Vertical profile of the cloud centre, derived from EDM measurements. **(b)** Particle concentration in an ideally shaped cloud. **(c)** Particle start positions for Itpas.

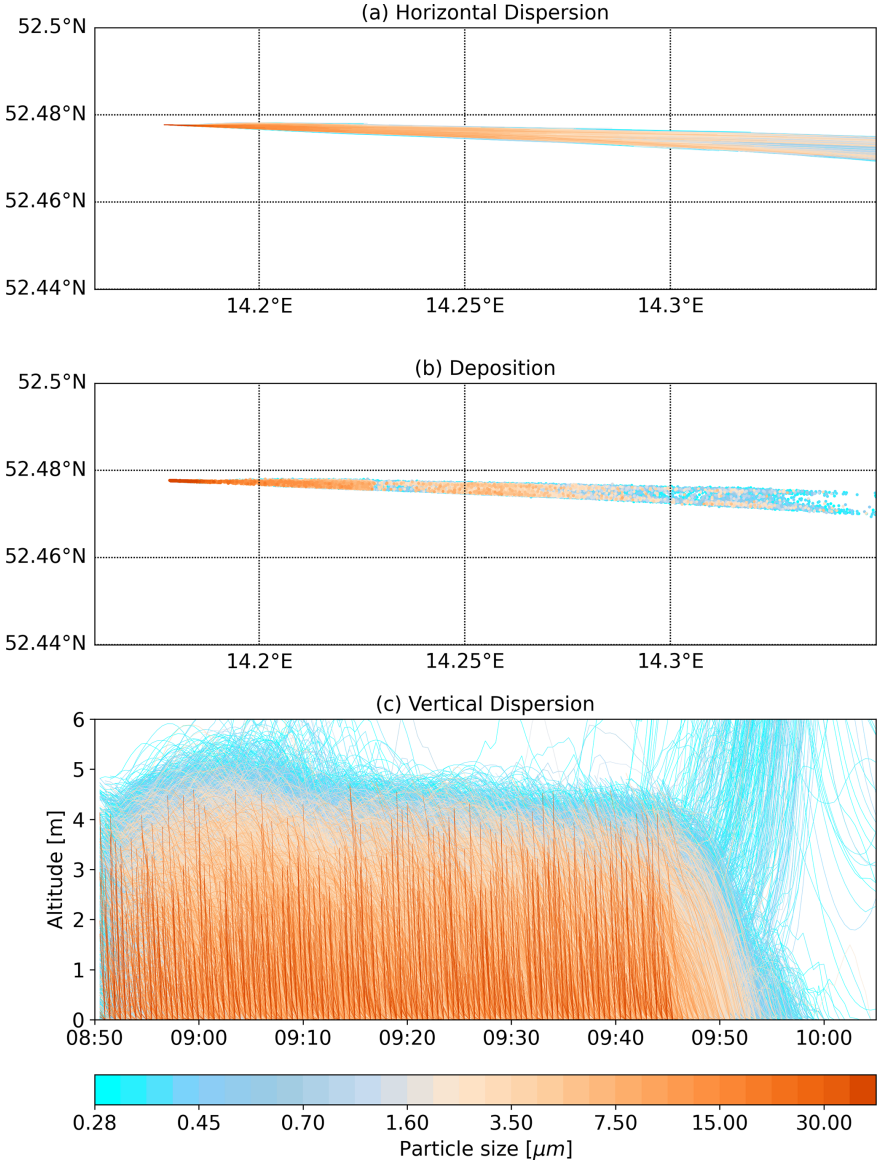

Figure 4. Particle motion of EXP1: **(a)** horizontal trajectories, **(b)** deposition points, **(c)** vertical trajectories.

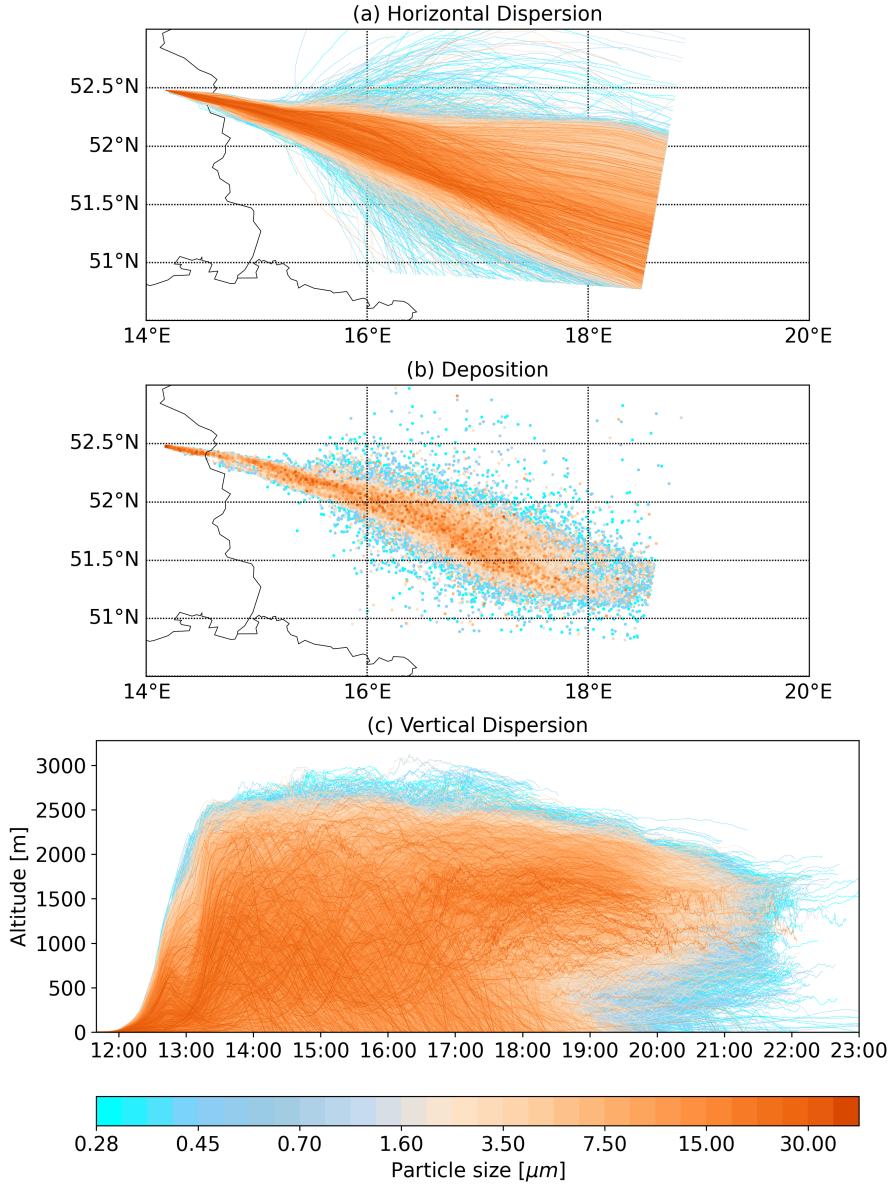

Figure 5. Particle motion of EXP2: **(a)** horizontal trajectories, **(b)** deposition points, **(c)** vertical trajectories.

altitude of the particles as a function of time, so it visualises the vertical dispersion and mixing of the particles. The colour indicates the particle size ranging from sub-micron particles in light blue to the coarse particles in orange. Please note that smaller particles are overlaid by the larger ones.

In the first experiment, the range of the particle transport was limited to the local surrounding (Fig. 4a). The vast majority of particles have not left this area so that the longest trajectories have a length of about 10 km. The particles spread only a few hundreds of metres in the direction perpendicular to the mean wind . The deposition map (Fig. 4b) shows a colour gradient from west to east, which indicates the coarse particles depositing close to the source while smaller particles are able to travel longer distances. This becomes even clearer from time series of the vertical dispersion (Fig. 4c). Please note that the altitude axis is restricted to 6 m. The particles were not lifted into higher levels and fell down more or less quickly after entrainment depending on their size. At the upper edge of the plume, it is visible that the smallest particles, shown in light blue, form a kind of wave-like structure, which is linked to the random fluctuation that every particle experiences. Because of gravity forces, the amplitude of these waves becomes smaller with increasing particle size and disappears totally for the heavy particles that fall down directly. At the end of the displayed time range, individual particles experience an upward movement and travel further

on. These particles perform a similar movement to the particles in EXP2.

Only a brief look at Fig. 5 is necessary to notice that the situation changes drastically in EXP2. Beginning again with the horizontal dispersion (Fig. 5a) it is evident that the particles are going into long-range transport mode. The particles drift evenly apart as they cross the German–Polish border. Above western Poland ($\sim 15.5°$ E), the spread of the trajectories widens and thus the area covered by the particle plume (sum of the trajectories) increases significantly. Particularly affected hereof are the small particles (shown in light blue colour shades) which partly deviate strongly from the centre of the plume. The trajectories terminate above central Poland where the edge of the simulation domain is located. The most obvious feature on the deposition map (Fig. 5b) is the tendency of the small particles to spread further away from the core plume than the large particles do. But more interesting are the locations where the large particles deposit. It is apparent that these particles tend to fall down early during their journey. An indication for this is the dark orange stripe from the source to the German–Polish border (Fig. 5b). But also further on over Poland, a remarkable amount of dark orange dots can be found on the deposition map. This is an indication of an efficient vertical transport that was able to uplift the coarse-mode particle fraction. The particle uplift (Fig. 5c) can be described by three phases: the first phase is characterised by the emission of the dust particles (11:40–12:30 UTC), during which the particles slowly rise up to a couple of hundreds of metres above ground level. Then, at around 12:20 UTC, the particles experienced a strong uplift onto a level of 1200 m (second phase), visible as a shoulder in the uplifting trajectory pattern (cf. Fig. 5c). Finally, the particles experience a second strong lifting up to 2500 m above ground at around 13:00 UTC (third phase). The upper edge of the plume can clearly be identified as the top of the boundary layer. During the afternoon, the particles were mixed over the whole depth of the ABL. At 18:00 UTC (local time: UTC+2) again a transition in the distribution pattern is visible. Below 800 m altitude the particles slowly sink to the ground while the ones above this height start to travel on constant levels with strongly reduced vertical mixing. This process forms the overhanging lip of the vertical pattern in the last third of the plot.

4 Discussion

4.1 Model results

To completely understand the behaviour of Itpas, it is necessary to have a look into the atmosphere that was produced by COSMO, as illustrated in Fig. 6. It shows a temporal cross section through the atmosphere or, more precisely, the air column at the mean particle position. During the morning, this is the start point of the plume (the short-range transport from EXP1 is ignored). During the afternoon, the displayed air column follows a mean trajectory from the plume of EXP2. The mean trajectory travels in the centre of the particle plume and reaches the eastern edge of the model domain around 21:30 UTC. For the remaining time it rests at its terminal position. The altitude of the mean trajectory is marked in the plot as a red line together with the standard deviation in pale red. The main variable displayed in the cross section is the virtual potential temperature θ_v in colour shades from deep blue to dark orange. θ_v is a combined measure of temperature and moisture, weighted with the level height. Therefore it is well suitable to classify the atmospheric stratification. Vertically increasing values of θ_v indicate stable decreasing values unstable stratification. Figure A1 in the Appendix section shows the θ_v profile for the consecutive hours of the day and may help to interpret Fig. 6.

A closer look into the near-surface atmospheric conditions helps to understand the model behaviour in the morning hours (EXP1), during which the particles were not able to rise. A detailed view on the bottom-most 50 m can be found in the upper left corner of Fig. 6. Here, it is visible that θ_v increases at the levels above the surface and forms a small stripe of stable stratification. In a stable atmosphere, the vertical motion is inhibited, so no momentum is available to uplift the particles. During the morning hours, the vertical θ_v gradient becomes weaker and disappears until noon. But not only the atmospheric stratification is important for the vertical mixing, the overall driver of turbulent momentum is still the TKE. Now, focusing on the main plot of Fig. 6, the available TKE is drawn in dark grey isolines. The hours of emission during the different experiments are marked in green on the time axis. Besides the limited vertical motion, there is no TKE available at the beginning of EXP1, although a slight increase in the TKE during the end of EXP1's emission time occurs, which may provide enough momentum to push single particles upwards out of the stable surface layer (cf. Fig. 4c). However, even if the vertical particle motion in EXP1 behaves reasonably, the horizontal movement of the particles should be interpreted carefully. In the simulation, within a radius of up to 10 km around the source, the particles are uplifted less than 5 m above the surface. This close to the ground level, the COSMO model cannot provide reliable information of the horizontal wind do to its vertical resolution. Furthermore, the spatial grid resolution of 2.8 km is relatively coarse compared to the travel range (10 km). Additionally, small surface structures like buildings, trees or forests are not included in the simulation. Thus, EXP1 should be considered as a case without particle transport. In essence, the dust particles emitted by the tractor are whirled up but then deposited soon after emission.

Later during the day for EXP2, we can see changes in both the near-surface TKE and the θ_v profile. At noon, a decrease in θ_v up to a height of at least 500 m is notable, which indicates unstable conditions in this layer. This allows the particles to rise, whereby the TKE induces the vertical

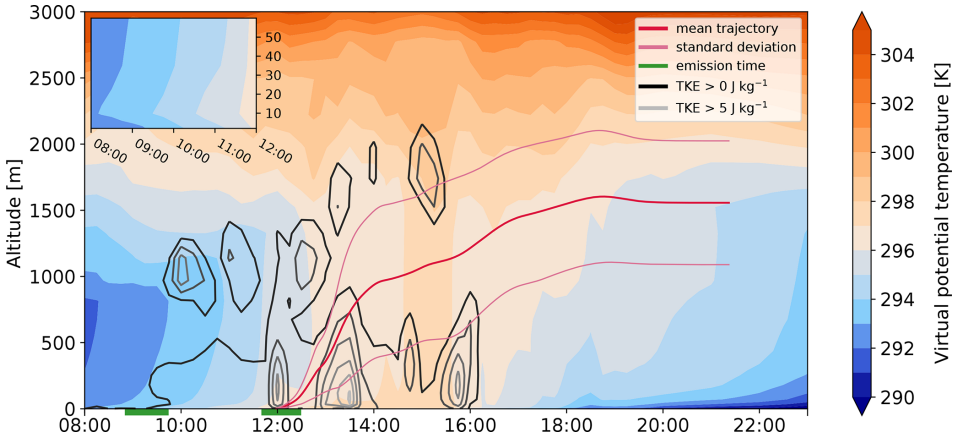

Figure 6. Atmospheric conditions for the particle dispersion. Cross section of the virtual potential temperature and TKE along the mean particle position of both experiments.

mixing. During the afternoon, the unstable layer extends up to 2000 m. Above 2500 m a strongly increasing gradient of θ_v indicates the top of the ABL. This gradual development of the ABL can also be observed from the trajectories (cf. Fig. 5c between 12:00 and 13:00 UTC).

Between 13:00 and 14:00 UTC, the lower half of the particles (below the mean trajectory) passes a region with strongly increased TKE and the particles build momentum which enables them to shear out strongly from the main plume. This situation corresponds spatially and temporally to the enhanced spreading of the trajectory plume above western Poland (cf. Fig. 5a).

After 16:00 UTC the temperature at the surface is decreasing and the ABL collapses forming the transition into a nocturnal boundary layer structure: a stable surface layer forms which deepens during the evening into the typical stable nocturnal boundary layer. The particle plume gets divided into two parts, one remaining within the stable ABL and one above. Similar to the particles in EXP1 the part of the plume inside the stable nocturnal boundary layer lacks all turbulent momentum keeping the particles aloft, and, ultimately, the particles settle down. Only these particles within the residual boundary layer above the nocturnal boundary layer remain airborne. In general, the residual layer is neutrally stratified, the turbulent mixing is strongly reduced and the model uses the short approach (cf. Fig. 1). Thus, the particles are trapped in this layer overnight and propagate within the general air flow at almost constant altitude.

Our results above showed that the representation of the diurnal cycle of the ABL is vital to an accurate trajectory calculation. The approach presented here includes a TKE-based approach to account for the ABL's turbulent features. A closer look into the role of turbulence to the particle transport is provided in Fig. 7: for a reduced version of EXP2 with $\sim 30\,000$, we ran three different set-ups aiming at representing the role of the different components of the wind ultimately determining the particle's trajectory. In the first set-up (Fig. 7a) we suppressed all vertical particle motion – those of the mean wind as well as those of the turbulence. It is considered as a control case. Comparable to EXP1 all particles deposit directly after the emission. Please note that the altitude is limited to 6 m.

The second set-up shown in Fig. 7b focuses on the role of the mean wind and its ability to mix the emitted particles in the ABL. Therefore we suppressed the vertical turbulence for this set-up. We observe that the mean wind of the model alone is not able to induce the particles into the atmosphere. Only 7 particles (out of 30 000) get lifted up to 2000 m. Nevertheless, a glimpse of the role of the mean wind mixing to the particle trajectories can be caught. The particles perform waves with a length up to 1 h and large amplitudes. The origin of these waves are the changing up- and downwind regions in the convective ABL. We also observed this kind of wave in EXP2 (cf. Fig. 5c) and assign them to the mean wind. In the convective ABL, turbulence is skewed towards the upward transport since updrafts and downdrafts are not evenly distributed, which may result in an underestimation of the near-surface concentration (Cassiani et al., 2015). However, we estimate the influence of this effect to be small in our model due to the high-frequency wind information.

Figure 7c focused on the turbulent portion of the vertical mixing; the vertical mean wind is suppressed in this third set-up. From this figure it becomes evident that turbulence is essential for the entrainment of particles into the boundary layer. But it also becomes visible that the heavier particles accumulate in the lower ABL, since the turbulent fluctuation is not as strong as the convective updrafts. Hence, it results in a boundary layer that is not well-mixed. In sum, the artificial set-ups emphasise that both components are significant for a mixing of particles from the near surface in the ABL that conforms with the criteria for well-mixed from Thomson (1987). Our approach provides a good balance between these

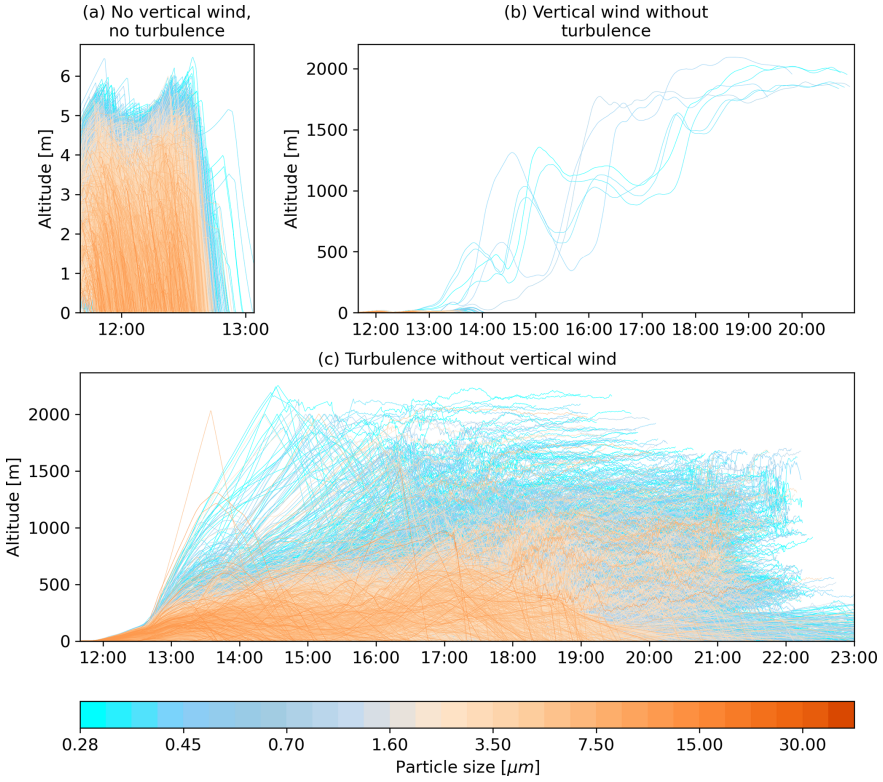

Figure 7. Vertical dispersion in an artificial set-up: **(a)** without vertical wind nor turbulence, **(b)** vertical wind only, **(c)** turbulence only.

components and therefore allows a realistic representation of the boundary layer dynamic in the particle trajectories.

4.2 Performance

COSMO uses the Message Passing Interface (MPI) for parallel computing on multiple processors, which divides the model domain into subdomains with each assigned to one computing process on a singe core. Thereby, a single process exclusively holds the information of its own subdomain, so it can only calculate a particle motion that is located in its own subdomain, and if a particle leaves a subdomain, it has to be passed to the next one. To handle this, we apply the strategy proposed by Miltenberger et al. (2013): during the iteration the process gathers all particles that leave the subdomain. At the end of the time step all particles leaving the subdomain get passed to their new subdomain in a single communication step. For an even number of particles in each subdomain, the model system would be able to process them in parallel. However, when the particles travel as a plume they are most probably assigned to a few or even only one subdomain. As a consequence, the calculation is performed quasi-serially. On the other hand, if we distribute the particles independently of their subdomain, we would also need to pass the atmospheric data for the calculation. This may result in a communication overhead. The efficient calculation of online trajectories remains a dilemma between communication and data availability. So further research is necessary on this technical aspect.

Our simulations were performed multiple times on different machines with 36 processors. For the simulation of EXP1 during which (nearly) all particles are deposited within the first minutes, the runtime was about 40 % longer than for a test case without particles. The simulation of EXP2 took roughly 10 times longer than the simulation without particles. On our most recent system (Intel(R) Xeon(R) Platinum 8160 CPUs; 2.10 GHz) the runtime of EXP2 was 260 min compared to 36 min for EXP1 and 25 min without particles.

5 Conclusions

Lagrangian particle dispersion models are widely used to study the pathway of air masses and associated aerosol plumes, e.g. those originating from volcanic eruptions, wildfires or desert storms. Building on the trajectory model (Miltenberger et al., 2013) coupled online to the German Weather Service's NWP model COSMO, we created the LPDM module Itpas in order to account for the turbulent nature of the convective daytime boundary layer. Here, we included the TKE on high temporal resolution, aiming for an improved representation of particle dispersion within the ABL. In order to showcase the strength of such an online coupled TKE-based approach, we simulate aerosol particle dispersion for

two cases (EXP1 and EXP2) of mechanically driven particle emission in northeastern Germany on 31 May 2017. The experiments are of particular interest as (1) the emission could be described by a source function obtained from measurements performed during the experiments; (2) particles were emitted during two different times of the day (morning and early afternoon) characterised by differently stratified boundary layers; and (3) transport within the atmospheric boundary layer. In a nutshell, these conditions are required to consider the air flow as non-linear and turbulent.

Simulating the particle dispersion for the emission events (EXP1 and EXP2), our results reflect the conceptual model of the boundary layer development throughout the day. Entrained into a rather stable and stratified ABL (morning hours), the particles reside only for a few minutes within the atmosphere. The bunch of trajectories launched at the source travels as a bundle with only little spreading. Finally, particles do not experience much uplift and settle down rather close to the source, within a radius of about 10 km. Compared to the morning experiment, particles entrained during the early afternoon into the convective daytime boundary layer experienced significant vertical updraft and eventually were mixed over the entire depth of the boundary layer. Travelling longer distances by remaining aloft due to turbulent updraft, the particle trajectory plume further highlights another feature of the conceptual model of the boundary layer development: the formation of the nocturnal boundary layer and the residual layer as the upper part of the former daytime boundary layer above. Dust particles situated within the nocturnal boundary layer deposit due to the lack of turbulent buoyancy, whereas particles suspended within the residual layer remain aloft. Trajectories representing the first group of particles will terminate during nighttime, whereas trajectories representing the latter group may continue travelling within the air flow.

In essence, particles entrained into a well-developed convective ABL will more likely be mixed deeper into the boundary layer, travel longer distances and reside longer within the atmosphere. This furthermore emphasises the need for the development of prognostic TKE-based LPDMs, in particular for studies on, for example, aerosol transport whose source is located within the atmospheric boundary layer. The further development and application of this approach clearly would benefit from a thorough data validation such as in an extensive measurement framework.

Our approach opens up the possibility of an improved simulation of dust emissions from agricultural activities such as tillage or harvest. These emissions occur mainly in weather conditions characterised by low wind speeds and affect an area several times larger than that by wind erosion. The identification of source areas and transport paths of agricultural dust thus remains an important task, to which the presented modelling approach can make an important contribution.

Appendix A

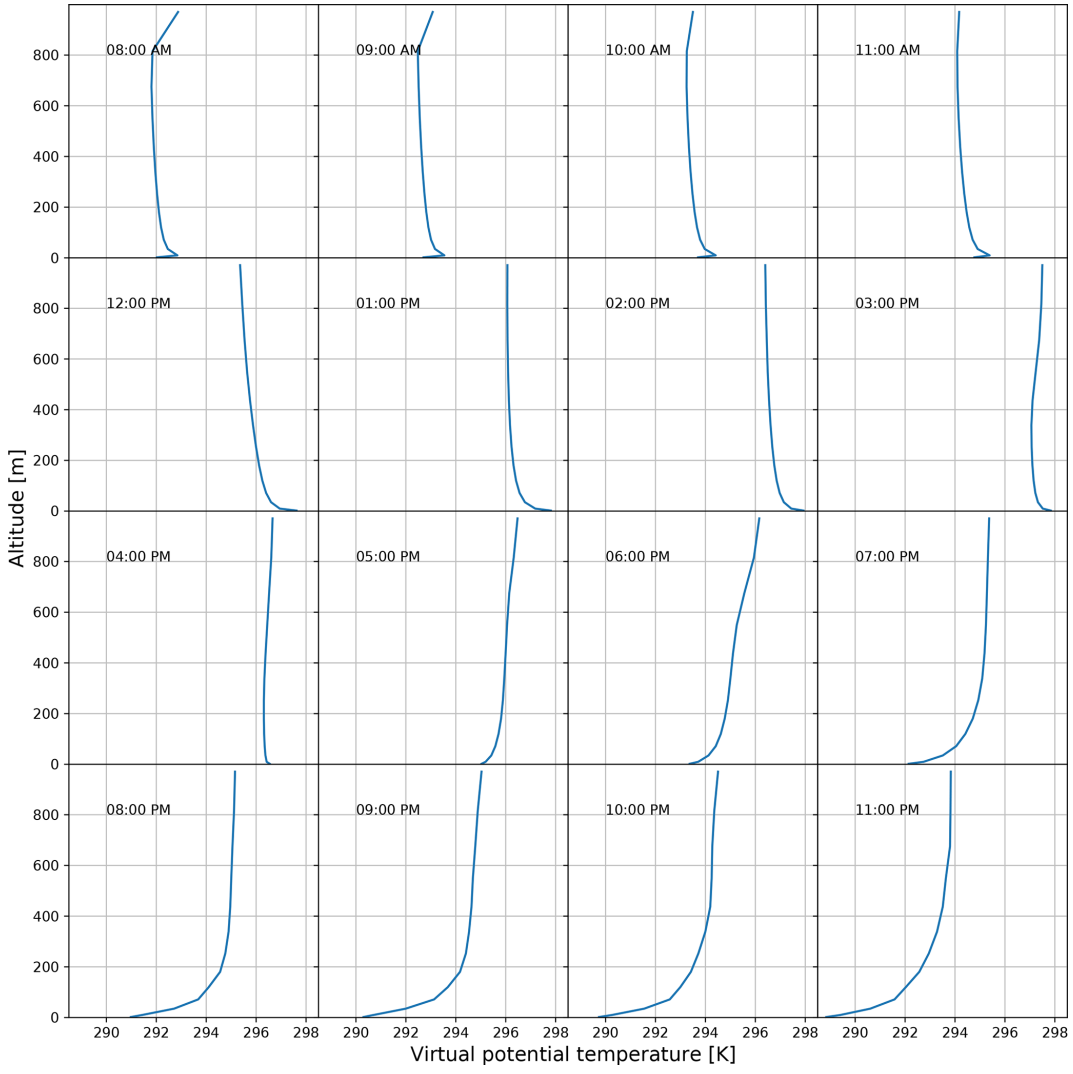

Figure A1. Vertical profiles of the virtual potential temperature along the mean trajectory of Fig. 6.

Code and data availability. The source code of the particle model Itpas is archived at Zenodo (https://doi.org/10.5281/zenodo.3932248, Faust, 2020a). Itpas is integrated into COSMO and the software is restricted to owners of a COSMO license. A free license for research purposes is available from the COSMO community (http://www.cosmo-model.org/content/consortium/licencing.htm, last access: 19 April 2021). For pre-processing, software for creating the particle source function is freely available (https://doi.org/10.5281/zenodo.3975563, Faust, 2020b). Software for processing, sorting and plotting of huge trajectory sets (https://doi.org/10.5281/zenodo.4062148, Faust, 2020c) and cross-section plots along trajectories (https://doi.org/10.5281/zenodo.4061940, Faust, 2020d) is openly accessible. A sample data set of Itpas' output is available at https://doi.org/10.5281/zenodo.3965682 (Faust, 2020e).

Supplement. The supplement related to this article is available online at: https://doi.org/10.5194/gmd-14-2205-2021-supplement.

Author contributions. The development of the introduced model Itpas and its pre- and post-processing resources, planning and execution of the model experiments, analysis of the model results, and design of the figures were done by MF. RW suggested the model development and evaluated the model physics. The measurements were obtained and analysed by SM and RF. KS supervised the study, suggested the model application, and contributed to the analysis of the model results and the structure of the paper. All authors contributed to the writing, editing and reviewing processes.

Competing interests. The authors declare that they have no conflict of interest.

Acknowledgements. We are grateful to the German Weather Service (Deutscher Wetterdienst, DWD) for making COSMO available to us and providing initial and boundary data. Furthermore we like to thank the two anonymous reviewers as well as P. Armand; their comments helped to improve this study. This study was carried out in the framework of the research project "Spread of antibiotics resistance in an agrarian landscape" (SOARiAL).

Financial support. This research has been supported by the Leibniz Association (grant no. SAW-2017-DSMZ-2).

The publication of this article was funded by the Open Access Fund of the Leibniz Association.

Review statement. This paper was edited by Slimane Bekki and reviewed by P. Armand and two anonymous referees.

References

Baldauf, M., Seifert, A., Förstner, J., Majewski, D., Raschendorfer, M., and Reinhardt, T.: Operational Convective-Scale Numerical Weather Prediction with the COSMO Model: Description and Sensitivities, Mon. Weather Rev., 139, 3887–3905, https://doi.org/10.1175/MWR-D-10-05013.1, 2011.

Borrelli, P., Lugato, E., Montanarella, L., and Panagos, P.: A New Assessment of Soil Loss Due to Wind Erosion in European Agricultural Soils Using a Quantitative Spatially Distributed Modelling Approach, Land Degrad. Dev., 28, 335–344, https://doi.org/10.1002/ldr.2588, 2016.

Brioude, J., Arnold, D., Stohl, A., Cassiani, M., Morton, D., Seibert, P., Angevine, W., Evan, S., Dingwell, A., Fast, J. D., Easter, R. C., Pisso, I., Burkhart, J., and Wotawa, G.: The Lagrangian particle dispersion model FLEXPART-WRF version 3.1, Geosci. Model Dev., 6, 1889–1904, https://doi.org/10.5194/gmd-6-1889-2013, 2013.

Cassiani, M., Stohl, A., and Brioude, J.: Lagrangian Stochastic Modelling of Dispersion in the Convective Boundary Layer with Skewed Turbulence Conditions and a Vertical Density Gradient: Formulation and Implementation in the FLEXPART Model, Bound.-Lay. Meteorol., 154, 367–390, https://doi.org/10.1007/s10546-014-9976-5, 2015.

Doms, G., Förstner, J., Heise, E., Herzog, H.-J., Mironov, D., Raschendorfer, M., Reinhardt, T., Ritter, B., Schrodin, R., Schulz, J.-P., and Vogel, G.: A Description of the Nonhydrostatic Regional COSMO Model, Part II : Physical Parameterization, Tech. rep., Consortium for Small-Scale Modelling, Deutscher Wetterdienst, https://doi.org/10.5676/dwd_pub/nwv/cosmo-doc_5.00_II, 2011.

Draxler, R. and Hess, G.: An overview of the HYSPLIT_4 modeling system for trajectories, dispersion, and deposition, Aust. Meteorol. Mag., 47, 295–308, 1998.

Faust, M.: In-time particle simulation (Itpas) module in the framework of the COSMO-Model, Zenodo, https://doi.org/10.5281/zenodo.3932248, 2020a.

Faust, M.: mttfst/dust-bubble: randomised test input, Zenodo, https://doi.org/10.5281/zenodo.3975563, 2020b.

Faust, M.: mttfst/trajectory-plot: Trajectory-Plot – Paper Version, Zenodo, https://doi.org/10.5281/zenodo.4062148, 2020c.

Faust, M.: mttfst/trajectory-cross-section: paper version, prep for sample data, Zenodo, https://doi.org/10.5281/zenodo.4061940, 2020d.

Faust, M.: In-time particle simulation (Itpas) – sample data, Zenodo, https://doi.org/10.5281/zenodo.3965682, 2020e.

Funk, R. and Reuter, H. I.: Wind Erosion, in: Soil Erosion in Europe, John Wiley & Sons, Ltd, 563–582, https://doi.org/10.1002/0470859202.ch41, 2006.

Funk, R., Reuter, H. I., Hoffmann, C., Engel, W., and Öttl, D.: Effect of moisture on fine dust emission from tillage operations on agricultural soils, Earth Surf. Proc. Landf., 33, 1851–1863, https://doi.org/10.1002/esp.1737, 2008.

Goossens, D.: Wind erosion and tillage as a dust production mechanism on North European farmland, in: Wind Erosion and Dust Dynamics: Observations, Simulations, Modelling, ESW Publications, Wageningen, the Netherlands, 15–40, 2004.

Goudie, A. S.: Desert dust and human health disorders, Environ. Int., 63, 101–113, https://doi.org/10.1016/j.envint.2013.10.011, 2014.

Hall, C. D.: The simulation of particle motion in the atmosphere by a numerical random-walk model, Q. J. Roy. Meteor. Soc., 101, 235–244, https://doi.org/10.1002/qj.49710142807, 1975.

Hanna, S. R.: Applications in Air Pollution Modeling, in: Atmospheric Turbulence and Air Pollution Modelling: A Course held in The Hague, chap. 7, Springer Netherlands, 275–310, https://doi.org/10.1007/978-94-010-9112-1_7, 1982.

Hinds, W. C.: Aerosol technology: properties, behavior, and measurement of airborne particles, John Wiley & Sons, New York, USA, 504 pp., 1999.

Holmén, B. A., James, T. A., Ashbaugh, L. L., and Flocchini, R. G.: Lidar-assisted measurement of PM_{10} emissions from agricultural tilling in California's San Joaquin Valley – Part I: lidar, Atmos. Environ., 35, 3251–3264, https://doi.org/10.1016/s1352-2310(00)00518-5, 2001.

Huneeus, N., Schulz, M., Balkanski, Y., Griesfeller, J., Prospero, J., Kinne, S., Bauer, S., Boucher, O., Chin, M., Dentener, F., Diehl, T., Easter, R., Fillmore, D., Ghan, S., Ginoux, P., Grini, A., Horowitz, L., Koch, D., Krol, M. C., Landing, W., Liu, X., Mahowald, N., Miller, R., Morcrette, J.-J., Myhre, G., Penner, J., Perlwitz, J., Stier, P., Takemura, T., and Zender, C. S.: Global dust model intercomparison in AeroCom phase I, Atmos. Chem. Phys., 11, 7781–7816, https://doi.org/10.5194/acp-11-7781-2011, 2011.

Joussaume, S.: Three-dimensional simulations of the atmospheric cycle of desert dust particles using a general circulation model, J. Geophys. Res., 95, 1909, https://doi.org/10.1029/jd095id02p01909, 1990.

Kim, K.-H., Kabir, E., and Kabir, S.: A review on the human health impact of airborne particulate matter, Environ. Int., 74, 136–143, https://doi.org/10.1016/j.envint.2014.10.005, 2015.

Kjelgaard, J., Sharratt, B., Sundram, I., Lamb, B., Claiborn, C., Saxton, K., and Chandler, D.: PM10 emission from agricultural soils on the Columbia Plateau: comparison of dynamic and time-integrated field-scale measurements and entrainment mechanisms, Agr. Forest Meteorol., 125, 259–277, https://doi.org/10.1016/j.agrformet.2004.04.004, 2004.

Legg, B. J. and Raupach, M. R.: Markov-chain simulation of particle dispersion in inhomogeneous flows: The mean drift velocity induced by a gradient in Eulerian velocity variance, Bound.-Lay. Meteorol., 24, 3–13, https://doi.org/10.1007/BF00121796, 1982.

Lemons, D. and Langevin, P.: An Introduction to Stochastic Processes in Physics, Johns Hopkins Paperback, Johns Hopkins University Press, Baltimore, USA, 128 pp., 2002.

Marx, A., Kumar, R., Thober, S., Rakovec, O., Wanders, N., Zink, M., Wood, E. F., Pan, M., Sheffield, J., and Samaniego, L.: Climate change alters low flows in Europe under global warming of 1.5, 2, and 3 °C, Hydrol. Earth Syst. Sci., 22, 1017–1032, https://doi.org/10.5194/hess-22-1017-2018, 2018.

Miltenberger, A. K., Pfahl, S., and Wernli, H.: An online trajectory module (version 1.0) for the nonhydrostatic numerical weather prediction model COSMO, Geosci. Model Dev., 6, 1989–2004, https://doi.org/10.5194/gmd-6-1989-2013, 2013.

Münch, S., Papke, N., Thiel, N., Nübel, U., Siller, P., Roesler, U., Biniasch, O., Funk, R., and Amon, T.: Effects of farmyard manure application on dust emissions from arable soils, Atmos. Pollut. Res., 11, 1610–1624, https://doi.org/10.1016/j.apr.2020.06.007, 2020.

Ngan, F., Stein, A., and Draxler, R.: Inline Coupling of WRF –HYSPLIT: Model Development and Evaluation Using Tracer Experiments, J. Appl. Meteorol. Clim., 54, 1162–1176, https://doi.org/10.1175/jamc-d-14-0247.1, 2015.

Ngan, F., Stein, A., Finn, D., and Eckman, R.: Dispersion simulations using HYSPLIT for the Sagebrush Tracer Experiment, Atmos. Environ., 186, 18–31, https://doi.org/10.1016/j.atmosenv.2018.05.012, 2018.

Panitz, H., Vogel, B., and Vogel, H.: The Lagrangian particle model traveling version 92/3. Model description and users' guide, KI-Topen, https://doi.org/10.5445/ir/270035362, 1994.

Pant, P. and Harrison, R. M.: Estimation of the contribution of road traffic emissions to particulate matter concentrations from field measurements: A review, Atmos. Environ., 77, 78–97, https://doi.org/10.1016/j.atmosenv.2013.04.028, 2013.

Petterssen, S.: Weather Analysis and Forecasting. Vol. 2 Weather Weather Systems, McGraw-Hill, New York, USA, 1956.

Pisso, I., Sollum, E., Grythe, H., Kristiansen, N. I., Cassiani, M., Eckhardt, S., Arnold, D., Morton, D., Thompson, R. L., Groot Zwaaftink, C. D., Evangeliou, N., Sodemann, H., Haimberger, L., Henne, S., Brunner, D., Burkhart, J. F., Fouilloux, A., Brioude, J., Philipp, A., Seibert, P., and Stohl, A.: The Lagrangian particle dispersion model FLEXPART version 10.4, Geosci. Model Dev., 12, 4955–4997, https://doi.org/10.5194/gmd-12-4955-2019, 2019.

Samaniego, L., Thober, S., Kumar, R., Wanders, N., Rakovec, O., Pan, M., Zink, M., Sheffield, J., Wood, E. F., and Marx, A.: Anthropogenic warming exacerbates European soil moisture droughts, Nat. Clim. Change, 8, 421–426, https://doi.org/10.1038/s41558-018-0138-5, 2018.

Seibert, P.: Convergence and Accuracy of Numerical Methods for Trajectory Calculations, J. Appl. Meteorol., 32, 558–566, https://doi.org/10.1175/1520-0450(1993)032<0558:caaonm>2.0.co;2, 1993.

Stein, A. F., Draxler, R. R., Rolph, G. D., Stunder, B. J. B., Cohen, M. D., and Ngan, F.: NOAA's HYSPLIT Atmospheric Transport and Dispersion Modeling System, B. Am. Meteorol. Soc., 96, 2059–2077, https://doi.org/10.1175/bams-d-14-00110.1, 2015.

Stohl, A.: Computation, accuracy and applications of trajectories – A review and bibliography, Atmos. Environ., 32, 947–966, https://doi.org/10.1016/s1352-2310(97)00457-3, 1998.

Stohl, A. and Thomson, D. J.: A Density Correction for Lagrangian Particle Dispersion Models, Bound.-Lay. Meteorol., 90, 155–167, https://doi.org/10.1023/A:1001741110696, 1999.

Stohl, A., Forster, C., Frank, A., Seibert, P., and Wotawa, G.: Technical note: The Lagrangian particle dispersion model FLEXPART version 6.2, Atmos. Chem. Phys., 5, 2461–2474, https://doi.org/10.5194/acp-5-2461-2005, 2005.

Stull, R.: An Introduction to Boundary Layer Meteorology, in: Atmospheric and Oceanographic Sciences Library, Springer Netherlands, Dordrecht, the Netherlands, 2012.

Taiwo, A. M., Harrison, R. M., and Shi, Z.: A review of receptor modelling of industrially emitted particulate matter, Atmos. Environ., 97, 109–120, https://doi.org/10.1016/j.atmosenv.2014.07.051, 2014.

Taylor, G. I.: Diffusion by continuous movements, Proc. London Math. Soc, 20, 196–212, 1922.

Tegen, I., Harrison, S. P., Kohfeld, K., Prentice, I. C., Coe, M., and Heimann, M.: Impact of vegetation and preferential

source areas on global dust aerosol: Results from a model study, J. Geophys. Res.-Atmos., 107, AAC 14-1–AAC 14-27, https://doi.org/10.1029/2001jd000963, 2002.

Thiel, N., Münch, S., Behrens, W., Junker, V., Faust, M., Biniasch, O., Kabelitz, T., Siller, P., Boedeker, C., Schumann, P., Roesler, U., Amon, T., Schepanski, K., Funk, R., and Nübel, U.: Airborne bacterial emission fluxes from manure-fertilized agricultural soil, Microbial Biotechnology, 13, 1631–1647, https://doi.org/10.1111/1751-7915.13632, 2020.

Thomson, D. J.: Criteria for the selection of stochastic models of particle trajectories in turbulent flows, J. Fluid Mech., 180, 529, https://doi.org/10.1017/s0022112087001940, 1987.

Unidata: Network Common Data Form (netCDF) version 4.7.4, Boulder, CO: UCAR/Unidata [software], https://doi.org/10.5065/D6H70CW6, 2020.

Zhang, L., Gong, S., Padro, J., and Barrie, L.: A size-segregated particle dry deposition scheme for an atmospheric aerosol module, Atmos. Environ., 35, 549–560, https://doi.org/10.1016/s1352-2310(00)00326-5, 2001.